Oxygen Reduction Reaction on Pt and Pt Bimetallic Surfaces: A Selective Review

N. M. Marković, T. J. Schmidt, V. Stamenković* and *P. N. Ross*

Materials Sciences Division, Lawrence Berkeley National Laboratory, University of California, Berkeley, CA 94720 (US)

Received 28.03.2001, revised 20.06.2001

Abstract

In this review we selectively summarize recent progress, primarily from our laboratory, in the development of the oxygen reduction reaction (ORR) catalysis on well-defined surfaces. The focus is on two type of metallic surfaces: platinum single crystals and bimetallic surfaces based on platinum. The single crystal results provide insight into the effects of the platinum structure on the kinetics of the ORR, and create a fundamental link between the specific activity of Pt (rate per unit area) and particle size (for various particle shapes). The results show that the structure sensitive kinetics of the ORR arise primarily due to structure sensitive adsorption of anions. In the absence of specific adsorption, such as in Nafion polymer electrolyte, no particle size effect is expected. The knowledge of the electrocatalysis of the ORR on model bimetallic surfaces on Pt-Ni and Pt-Co bulk alloys was used to resolve the enhanced ORR kinetics on supported Pt-Ni and Pt-Co catalysts. Finally, we show that the ORR on platinum modified with pseudomorphic Pd metal film in alkaline solution is the best catalysts ever used in O_2 reduction. For both bimetallic systems, we demonstrated that the ability to make a controlled and well characterized arrangement of two elements in the electrode surface region presage a new era of advances in the ORR electrocatalysis.

1 Introduction

In spite of many attempts in the last decade by researchers and fuel cell developers to create a non-Pt catalyst for low temperature (< 200 °C) air cathodes, Pt remains the catalyst of choice at least for acid-based fuel cells. Therefore, much of the art and science of catalysts development for the ORR rely on both the fundamental understanding of the reaction at the platinum-electrolyte interface [1-4] and the optimization of the catalytic properties of the platinum surface [5,6]. Our approach is to start with model systems, such as single crystal electrodes, in order to create a link between the microscopic level of understanding of surface processes and the macroscopic measurement of the kinetic rates of electrochemical reactions. This knowledge can be used to create tailor-made surfaces with improved catalytic activity. The optimization of the most promising catalysts must incorporate both non-catalytic and catalytic factors. The non-catalytic factors include either partial replacement of platinum catalysts with less noble metals, or the maximization of the catalyst surface area while exposing the most active microstructures. This, in turn, will minimize the amount (and cost) of catalysts required for a given level of activity. The catalytic factors include the modification of the intrinsic activity of platinum, usually by making bimetallic surfaces. The enhancement of catalytic properties by the second component may occur through the change of the local bonding geometry (structure effects), the distribution of active sites (ensemble effects) or directly by modifying the reactivity of platinum surface atoms (electronic effects). In real systems, all of these factors may, in general, operate simultaneously, thus, separating these effects and assessing their relative importance in the catalytic activity and reaction mechanism is a very challenging problem.

In this paper, we summarize recent progress, primarily from our laboratory, in the development of the ORR catalysis on well-defined platinum surfaces. The focus will be on two type of metallic surfaces: platinum single crystals and bimetallic surfaces based on platinum. The single crystal results provide insight into the effects of the platinum structure on the kinetics of the ORR, and create a fundamental link between the specific activity of Pt (rate per unit area) and parti-

[*] *Corresponding author, nmmarkovic@lbl.gov*

 1615-6846/01/0207-105 $ 17.50+.50/0

cle size (for various particle shapes). If the rate of the ORR on Pt is independent of particle size, then in practice one wants to achieve and maintain in use the highest possible dispersion, where all Pt atoms are surface atoms. There are a variety of physical forms that could be used to achieve such dispersion, but the thermodynamically favored shape is a facetted pseudosphere on the order of 1 nm in diameter. On the other hand, if the rate of the ORR varies with particle size and/or shape, then there are not only interesting fundamental questions raised as to why such a variation would occur, *i.e.,* the "crystallite size effect" [6], but a practical issue of "building" and maintaining in use the optimum particle size and/or shape. In practice, finding the optimum form of the Pt catalyst becomes a much more complicated task because of this extra variable. In the next two sections we focus on the inhibitive effects of trace levels of Cl_{ad} and Cu^{2+} on the kinetics of the ORR. Considering that high-surface area catalysts are often synthesized from halide-containing educts [7-12] and that trace levels of chloride may also be present in the water contained in the feed-stream, the effect of Cl^- is of particular practical importance. Trace levels of copper may also be present in the real system, mostly as a corrosion product, thus the effects of underpotentially deposited copper (Cu_{upd}) on Pt(hkl) will serve as a model system to understand why a small amount of copper has a devastatingly inhibiting effect on the ORR. The last two sections are devoted to the enhanced kinetics of the ORR on Pt-Ni and Pt-Co bulk alloys and on platinum single crystals modified by a thin Pd metal film. We demonstrate that the ability to make a controlled and well characterized arrangement of two elements in the electrode surface region presage a new era of advances in the ORR electrocatalysis.

2 Experimental

All measurements were carried out by making use of the rotating ring-disk electrode (RRDE) technique. The Pt single crystals and polycrystalline Pt_3M alloy (M = Ni, Co) electrodes were prepared either by the flame annealing technique [13,14] or in ultra-high vacuum by sputtering/annealing cycles, respectively. After preparation, the electrodes were transferred into the disk position of an insertable ring-disk arbor as described in ref. [15]. Before the transfer, the Pt_3M alloys were characterized in UHV by Auger electron spectroscopy (AES) and Low Energy Ion Scattering (LEIS). Details about the UHV preparation and characterization of Pt alloy crystals can be found in ref. [16,17]. LEIS revealed that the surface composition of the Pt_3M alloy electrodes equaled the bulk composition, *i.e.*, the surface consists of 75 % Pt and 25 % of the alloying component [17]. Details about the preparation of the Pd-modified Pt(hkl) electrodes can be found in ref. [18].

For measurements with the high-surface area catalysts, we used the thin-film RDE method [19]. For details about the preparation of the thin-film electrode, the reader is referred to ref. [19,20]. We investigated a commercially available Pt catalyst (20 wt% platinum supported on Vulcan XC72), two Pt-Co-alloy catalysts (20 wt% PtCo/Vulcan XC72, a/o = 1/1, and 20 wt% Pt_3Co/Vulcan XC72, a/o = 3/1), and a Pt_3Ni/Vulcan XC72 (20 wt%, a/o = 3/1) catalyst (E-Tek). To avoid any misunderstanding we will refer to these catalysts as to Pt/Vulcan, PtCo/Vulcan, Pt_3Co/Vulcan, and Pt_3Ni/Vulcan respectively. All potentials in this manuscript refer to that of the reversible hydrogen electrode. For experimental details about our measurements, we refer to ref. [15,17-24].

3 ORR at the Pt(hkl) surfaces

Interest in the role of the local symmetry of platinum surface atoms in electrocatalysis has risen steadily over the last three decades. Ever since the pioneering work of Will [25], one of the major themes in electrochemical research has been the study of the relationship between the electrochemical reactivity and surface structure, a functionality generally termed "structural sensitivity". The recent advances in the *in-situ* methods of surface x-ray scattering (SXS) [26,27] have made it possible to establish the true relationship between the kinetics of electrochemical reactions and surface structure of platinum single crystal surfaces [4]. As we demonstrate below, the crystallite size effect for the ORR reported for supported Pt catalysts in sulfuric acid solution may be explained by applying the single crystal results to a classical model of the variation in particle shape with size. The presentation here will be restricted to a relatively brief overview of the science; further details, including experimental procedures, can be found in the references cited.

3.1 Reaction pathway

Oxygen reduction reaction is a multielectron reaction that may include a number of elementary steps involving different reaction intermediates. Of various reaction schemes proposed for the ORR [6], a modified Wroblowa *et al.,* [28] scheme appears to be the most effective one to describe the complicated reaction pathway by which O_2 is reduced at metal surfaces:

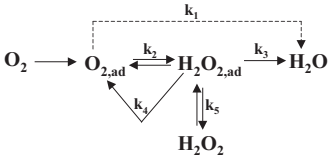

Based on this reaction scheme, O_2 can be electrochemically reduced either directly to water with the rate constant k_1 without intermediate formation of $H_2O_{2,ad}$ (so-called "direct" $4e^-$ reduction) or to $H_2O_{2,ad}$ with the rate constant k_2 ("series" $2e^-$ reduction). The adsorbed peroxide can be electrochemically reduced to water with the rate constant k_3 ("series" $4e^-$ pathway), catalytically (chemically) decomposed on the elec-

trode surface (k_4) or desorbed into the bulk of the solution (k_5). Although a number of important problems pertaining to the interpretation of the reaction pathway for the ORR on Pt(hkl) have yet to be resolved, recent studies presented from our laboratory [21,29,30] suggest that a "series" pathway *via* an $(H_2O_2)_{ad}$ intermediate may be operative on Pt and Pt bimetallic catalysts. This can be considered as a special case of the general mechanism where k_1 is essentially zero, *i.e.*, there is no splitting of the O-O bond before a peroxide species is formed. Peroxide, on the other hand may (k_5=0) or may not ($k_5 \neq 0$) be further reduced to water. In either case, the rate determining step appears to be the addition of the first electron to $O_{2,ad}$. The rate expression is then [2,30-32],

$$i = nFKc_{O_2}(1-\Theta_{ad})^x \exp(-\beta FE/RT)\exp(-\gamma r\Theta_{ad})/\mathrm{RT} \quad (1)$$

where n is the number of electrons, K is the chemical rate constant, c_{O_2} is the concentration of O_2 in the solution, Θ_{ad} is the total surface coverage by all adsorbed species, x is either 1 or 2 depending on the site requirements of the adsorbates, i is the observed current, E is the applied potential, β and γ are the symmetry factors (assumed to be ½), and $r\Theta_{ad}$ is parameter characterizing the rate of change of the apparent standard free energy of adsorption with the surface coverage by adsorbing species. Assuming that the coverage of ORR intermediates is small under reaction conditions [31], for most cases, only two adsorbed species need to be considered, OH_{ad} and specifically adsorbing anions like (bi)sulfate or halides. In the following sections, we will use this reaction pathway and rate expression to analyze the effects of various factors on the kinetics of the ORR on Pt(hkl) surfaces.

3.2 Structure sensitivity of the ORR and implications for crystallite size effects

It is now well established that the reaction rates of the ORR on Pt(hkl) surfaces are a structure sensitive [33,34] which arise due to structure sensitive adsorption of spectator species, such as H_{upd} [15,34], OH_{ad} [35], $HSO_{4(ad)}$ [15], Cl_{ad} [21], and Br_{ad} [30]. Within the limited scope of this report, it will not be possible to review all of these results. Rather we will show, using representative examples, the kind of information that can be used to improve our understandings of the role of the local symmetry of platinum surface atoms in the O_2 reduction electrocatalysis. There are two general observations concerning the structure sensitivity of the ORR: (i) the *same* activation energy in both acid (at the reversible potential *ca.* 42 kJ/mol [29]) and alkaline solution (at 0.9 V *ca.* 40 kJ/mol [36]) has been found for all three Pt(hkl) surfaces; (ii) the structural sensitivity is most pronounced in electrolytes in which there is strong adsorption of anions. At the Pt(111)-$HSO_{4(ad)}$ [15], Pt(hkl)-Cl_{ad} [21], and Pt(hkl)-Br_{ad} [30] interfaces a single Tafel slope of *ca.* 120 mV/dec is deduced from the kinetic analyses of the results for ORR on Pt(hkl). This appears to be consistent support that the standard free energies of adsorption of the reaction intermediates are not affected by the adjacent anions and thus the term $r\Theta_{ad}$ becomes a constant factor. As a consequence, the structure sensitivity in the solution containing bisulfate and halide anions is *completely* determined by the availability of free Pt sites, the $(1-\Theta_{ad})$ coverage dependent term.

For the purpose of demonstrating the importance of the $(1 - \Theta_{ad})$ term in the kinetics of the ORR on Pt(hkl), two representative sets of polarization curves are shown in Figure 1. Figure 1a shows that the ORR in H_2SO_4 increases in the sequence Pt(111) < Pt(100) < Pt(110) [37]. An exceptionally large deactivation is observed at the Pt(111) surface. This is probably due the strong adsorption of the (bi)sulfate anion from the symmetry match between the *fcc* (111) face (see insert of Figure 1) and the C_{3v} geometry of the oxygen atoms of the sulfate anion [38]. The fact that the activity of all three low-index platinum planes is significantly higher in $HClO_4$ [4] does, however, suggest that adsorption of (bi)sulfate anions effects the kinetics of the ORR on all three surfaces, but particularly strong on Pt(111). It should be noted that although bisulfate adsorption onto Pt(hkl) surfaces inhibits the reduction of molecular O_2, most likely by blocking the initial adsorption of O_2, it does *not* affect the pathway of the reaction, since no H_2O_2 is detected on the ring electrode for any

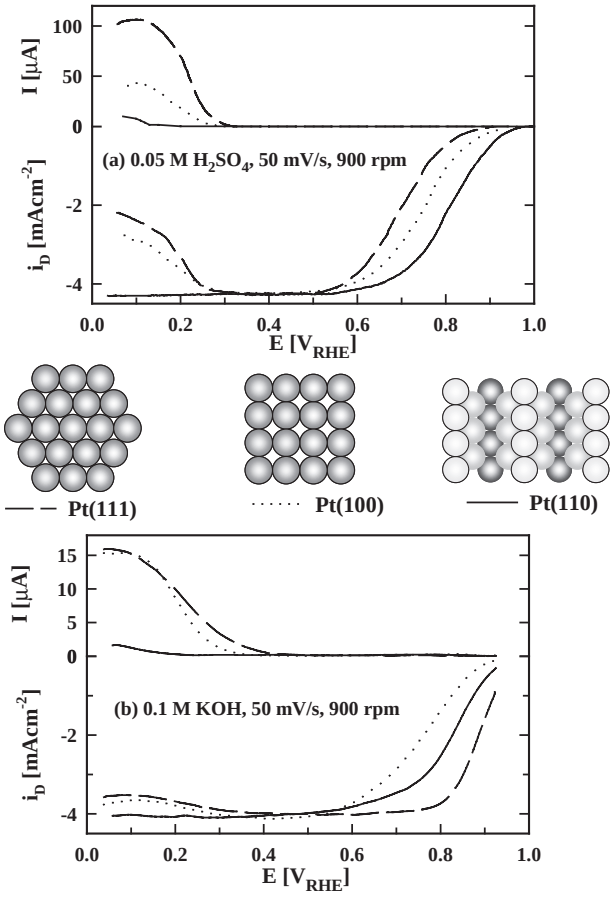

Fig. 1 **(a)** Oxygen Reduction on Pt(hkl) in 0.05 M H_2SO_4 (50 mV/s, 900 rpm, 298 K), lower part, disk currents; upper part, ring currents. **(b)** Oxygen Reduction on Pt(hkl) in 0.1 M KOH (50 mV/s, 900 rpm, 298 K), lower part, disk currents; upper part, ring currents. **Insert**: Surface structure of Pt(111), Pt(100), and Pt(110), respectively.

of the surfaces in the kinetically controlled potential region (Fig. 1a).

The first correlation between the kinetics of the ORR and the surface coverage of chemisorbed oxygen-containing species, historically termed "oxide", was established on a polycrystalline platinum electrode. In this study Tarasevich [31] proposed that both transition in the Tafel slope and the adsorption of O_2 is controlled by the surface coverage of chemisorbed oxygen-containing species. Very recently, by eliminating the surface heterogeneity of a polycrystalline Pt electrode with single crystal electrodes, Markovic et al., [4] gained new insight into the relationships between the surface coverage of platinum "oxides" and the kinetics of the ORR. We note that single crystal work clearly showed that two different types of chemisorbed oxygen-containing species occur on platinum, a reversible form (denoted hereafter as OH_{ad}) and irreversible form, which we shall call "oxide" hereafter. The most direct probe of the effects of OH_{ad} on the ORR kinetics can be obtained in alkaline solution, since no other anions are co-adsorbed with hydroxyl species. Figure 1b shows that in the potential range where O_2 reduction is under combined kinetic-diffusion control (E > 0.75 V), the order of activity of Pt(hkl) in 0.1M KOH increase in the sequence (100) < (110) < (111) [35]. As already discussed in [35], the structure-sensitivity of the ORR in this potential region arise due to the structure sensitive adsorption of the hydroxyl species. It is interesting that although the reversible adsorption of hydroxyl ions (OH_{rv}) on Pt(hkl) suppresses the kinetics of the ORR, it does not affect the pathway of the reaction since peroxide is not detected on the ring electrode for any of the surfaces in the potential range where the reversible form of OH_{ad} is present on the surface. In contrast, irreversibly adsorbed "oxide" does change the reaction pathway, *i.e.*, peroxide is detected at the ring when there is a significant amount of this form on the surface, as seen in the negative going sweeps on (100) and (110) [35]. Note that the ORR is more strongly inhibited by OH_{ad} which is adsorbed on the Pt(100) surface than on two other single crystal surfaces, Figure 1b. This is possibly related to a high affinity of the (100) sites (insert of Figure 1) for the hydroxyl adsorption and the lack of active centers for the O_2 adsorption on highly covered Pt(100) with OH_{ad}. Although at the same overpotentials the apparent surface coverage by adsorbed OH_{ad} on Pt(110) is similar [35], if not slightly higher, than on Pt(100), the activity of Pt(110) is higher than the activity of Pt(100). If on the *fcc* (110) surface (insert of Figure 1) the adsorption of hydroxyl ion is predominantly in the "trough" positions, then the top atoms may serve as active centers for the ORR even when the Pt(110) surface is a "fully" covered with OH_{ad} [35].

The structure sensitivity of the ORR described above may provide some new insight into the particle size effects reported for the ORR using supported Pt catalysts. We note however, that there is no any single system that will model all the aspects of real catalysts; particularly in the exact configuration they are used in electro catalytic cells. Nevertheless, to begin pursuing any of highly structured nanoparticule concepts, well-characterized surfaces should be used as the most adequate model for real catalysts. Furthermore, the observations of structure sensitivity of the ORR are not as useful at present as they might be because the experimental conditions, *e.g.*, temperature and electrolyte, used in most ORR kinetic measurements with supported catalysts are not those employed in the RRDE measurements with single crystals. There is only one out of the many particle size effect studies that employed exactly the same conditions as those used here for single crystals: the study by Peukert et al. [39], who reported results in dilute sulfuric acid at ambient temperature. Fortunately, this was a very carefully done study using well-characterized supported Pt catalysts with (average) crystallite sizes ranging from 11.7 nm down to 0.78 nm. As shown by Kinoshita [6], the crystallite size dependence in the data of Peukart *et al.*, are essentially perfectly fit by a model which assumes: *i)* that only the (100) face is active for the ORR; and *ii)* that the Pt particles are perfect cubooctohedra. Below about 6 nm, the fraction of the surface having (100) facets drops rapidly, and actually goes to zero below 1.8 nm; particles below 2 nm are formed almost entirely from (111) facets and their intersections (edges and corners) [6]. Our ORR data from single crystal Pt in sulfuric acid fully support this model, since we have observed that the (100) face is more active by two orders of magnitude versus the (111) face (in the model calculations, a factor of 100 between the two faces is sufficient to fit the data [6]). By inference then, the crystallite size effect for the ORR on supported Pt in sulfuric acid at ambient temperature would be due to the structure sensitive adsorption of (bi)sulfate anions, this adsorption effectively eliminating the contribution of the (111) facets to the overall rate.

Kinoshita has also shown that ORR data for supported catalysts in hot, concentrated H_3PO_4 (180 °C, 97–98 % acid) reported in three different studies were also fit by this model [6]. Since the physical basis for the crystallite size effect in sulfuric acid is anion adsorption, it would be a reasonable to suggest that the same physical basis applies to this size effect, *i.e.*, structure sensitive anion adsorption. There are, nonetheless, indications that this is the case. Anion adsorption in dilute phosphoric has very similar structure sensitivity as sulfate adsorption [33]. Sattler and Ross [40] reported a similar crystallite size dependence of the ORR on supported Pt in dilute phosphoric acid at ambient temperature as that found in hot, concentrated acid with the same catalysts. But it is unclear whether similar adsorption chemistry would exist in the extreme conditions of hot, concentrated phosphoric acid. With differences in activity between crystal faces of only a factor of five or less for oxygen reduction in perchloric acid [41], the particle models of Kinoshita indicate that there would little or no crystallite size effect for the ORR in a non-adsorbing acid, such as, *e.g.*, trifluoromethane sulfonic acid or Nafion.

3.3 Effects of Cl_{ad}

3.3.1 Pt(hkl)

The family of polarization curves for the ORR on Pt(hkl) in 0.05 M H_2SO_4 + 10^{-3} M Cl^- are shown in Figure 2. The polarization curves for the ORR in pure 0.05 M H_2SO_4 solutions is shown for one rotation rate as a reference. A full description of the polarization curves for the ORR on Pt(111) in pure sulfuric acid solution is given in our previous publications [15]. In the presence of Cl^-, the variation in activity increases in the order (100) < (110) < (111) [21]. Figure 2a shows that the ORR on the Pt(111) surface in 0.05 M H_2SO_4 +10^{-3} M Cl^- is strongly inhibited, with an activity in a solution containing Cl^- being several orders of magnitude lower than in 0.05 M H_2SO_4 [21,33]. Figure 2a also shows that between 0.3 < E < 0.9 V, the ring currents were a small fraction of the disk currents, implying that on the surface highly covered with Cl_{ad} oxygen reduction proceeds almost entirely through the $4e^-$ reduction pathway. The appearance of peroxide oxidation currents on the ring electrode begins at potentials negative of 0.25 V, and parallels with the adsorption of hydrogen on Pt(111).

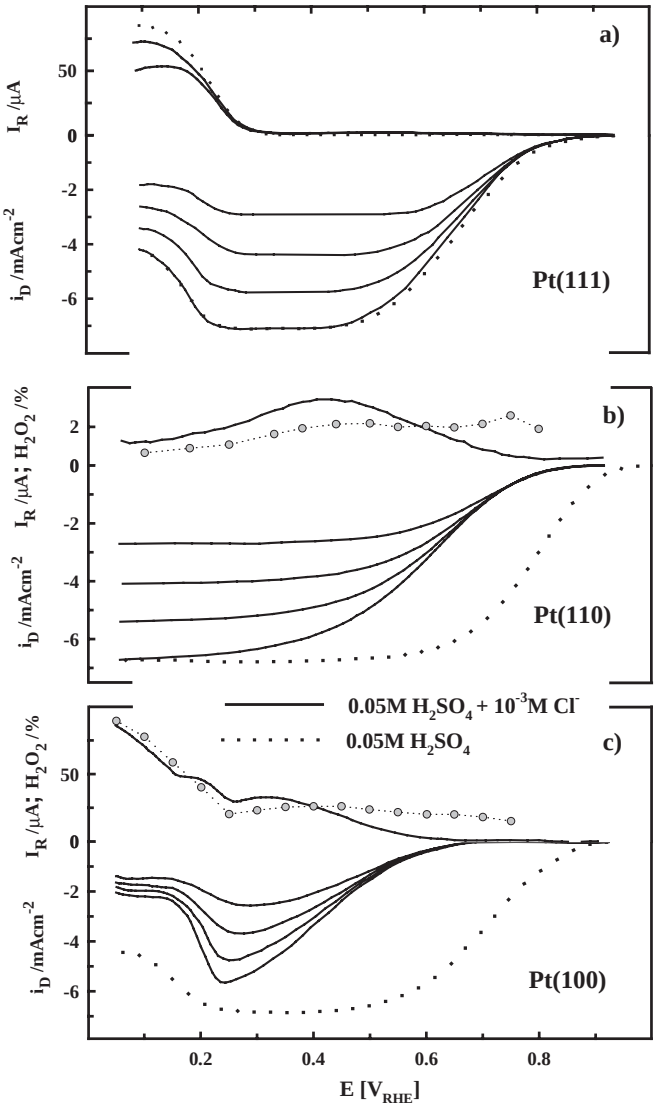

Fig. 2 Ring and Disk currents for the ORR in 0.05 M H_2SO_4 + 10^{-3} M Cl^- on **(a)** Pt(111) **(b)** Pt(110), and **(c)** Pt(100) at different rotation rates (full lines). The respective polarization curves on Pt(hkl) in 0.05 H_2SO_4 for 2500 rpm are shown as a reference (dotted line). The gray circles represents the fraction of peroxide formed during the ORR according to eq. 2. 50 mV/s, 293 K.

In contrast to Pt(111), the ORR on Pt(110) (Figure 2b) and Pt(100) (Figure 2c) in Cl^-containing solution is accompanied, but not quantitatively mirrored, with peroxide formation, implying that within the same potential limits H_2O_2 is formed as an intermediate on the Pt(110) and Pt(100) electrodes covered with Cl_{ad}. On Pt(100) the fraction of H_2O_2 produced between 0.25 < E < 0.6V during the ORR, calculated from Figure 2c using equation 2 [42],

$$x_{H_2O_2} = \frac{2I_r/N}{I_d + I_r/N} \qquad (2)$$

is almost constant and is close to 25% (note in this relation, N denotes the collection efficiency of the ring-disk configuration, I_d and I_r are the disk and ring currents, respectively). At potentials more negative than E = 0.3 V the surface coverage with Cl_{ad} is reduced substantially, but the O_2 reduction currents sharply decrease to diffusion limiting currents for ca. $2e^-$ per O_2 molecule at the negative potential limit. In the same potential region the O_2 reduction currents on the disk electrode are accompanied quantitatively by the H_2O_2 oxidation currents on the ring electrode, reaching maximum peroxide production of ca. 90% at 0.075 V. In Cl^--free solution, however, a $3e^-$ reduction is observed at the same potential limit [15]. This may suggest that Cl_{ad} is *always* present on Pt(100) covered by H_{upd}, thus the availability of Pt atoms required for the breaking of the O-O bond are significantly reduced and the ORR proceeds entirely through the $2e^-$ peroxide pathway on the Pt(100)-H_{upd}-Cl_{ad} surface. The amount of peroxide formed on the Pt(110) surface is substantially smaller, Figure 2b, *ca.* 2.5 %, and no increase in peroxide formation was observed in the H_{upd} region.

As we have demonstrated recently [21], the key to resolving the structural sensitivity of the ORR on the Pt(hkl) surfaces in Cl^- containing solution is to be found in understanding the relationships between the strength of the Pt-Cl_{ad} interaction, the specific type of sites for Cl_{ad}, and the effect of Cl_{ad} at these sites on the rate of O-O bond breaking and/or bond making. In particular, due to the strong interaction of Cl_{ad} with Pt(100) the ORR between 0.3 V and 0.75 V is inhibited and the number of platinum sites required for adsorption of O_2 and the breaking of O-O bond are reduced, which is in accord with the peroxide formation in the same potential region. In the case of Pt(110), although the interaction of Cl_{ad} with Pt(110) is as strong as with (100) sites, Cl_{ad} is most likely adsorbed in the "troughs" of the surface (insert of Figure 1), thus leaving the top sites available for O_2 adsorption and the cleavage of the O-O bond. Apparently, the Pt(111)-Cl_{ad} system has the same effect on the ORR as bisulfate anions, i.e., although Cl_{ad} inhibits the initial adsorption of O_2 molecules, it does *not* affect the pathway of the reaction, Figure 2a.

3.3.2 Supported catalysts

In developing the basis for discussing the effects of Cl^- in real catalysts systems, we start by summarizing the Tafel plots for the ORR on a Pt/carbon fuel cell catalyst [24]. Figure 3a shows the current versus potential curve for the ORR on Pt/Vulcan in 0.5 M $HClO_4$ with and without chloride. In accord with the ORR on Pt(hkl), the onset for the ORR is shifted to higher overpotentials with increasing chloride concentration in the solution. Compared to the ORR in the absence of Cl^- the activity at constant potential decreases roughly one order of magnitude for each order of magnitude increase in chloride anion concentration. In addition, considerable H_2O_2 currents on the ring electrode (Figure 3b) are observed in solutions containing Cl^-, *e.g.*, with increasing Cl^- concentration, the fraction of peroxide is increasing up to 10 % at $c_{Cl^-} = 10^{-3}$ M and 14 % at $c_{Cl^-} = 10^{-2}$ M around 0.6 V, respectively. As for the kinetics of the ORR on Pt(hkl) in the preceding section, Cl_{ad} has two effects in the kinetics of the ORR on a supported platinum catalyst: (i) Cl_{ad} acts as a site-blocking species which is reducing the number of active sites for the adsorption of O_2 molecules and (ii) Cl_{ad} is affecting the number of sites required for the breaking of the O-O bond. Therefore, the kinetic activity and the reaction pathway for the ORR on supported catalysts in the presence of Cl_{ad} is fully explained by applying the single crystal results to the relationship between particle size and the different surface sites (crystal faces, edges and corners) [6]. Based on a HRTEM analysis, the structure of typical Pt particle (mean particle size ca. 3.7 ± 1 nm [19]) illustrated in Figure 3 show clearly that the cubo-octahedral Pt nanoparticles close to the edge of the carbon support is facetted, exposing mostly (111) and (100) crystal faces and edges and corner sites with probable (110) symmetry. At the (111) facets Cl_{ad} acts exclusively as a site-blocking species without enhancing the formation of H_2O_2. In addition to blocking the adsorption of O_2, the (100) facets and (110) corner/edge sites are effecting the breaking of the O-O bond and, hence, the production of peroxide on a supported Pt catalysts, *ca.* 15%, is close to the average value of H_2O_2 produced on Pt(100) (*ca.* 25%) and Pt(110) (*ca.* 2.5%) single crystal surfaces.

3.3.3 Implications for PEM fuel cells

As shown in the aforementioned sections, even trace amounts of chloride (*i.e.*, 10^{-4} M Cl^- or ca. 4ppm) drastically change both the activity and the reaction pathway of the ORR on Pt catalysts. Although these results were obtained in liquid electrolyte, similar effects can be expected on electrodes in a solid-polymer electrolyte as present in a PEMFC. In this case, chloride impurities on the level of a couple of ppm, either due to incorporation into the MEA during preparation or due to contamination of the humidified fuel cell feed streams, will strongly affect the MEA performance. Based on the data in Figure 3, chloride contamination on the order of 4ppm would result in a fuel cell voltage loss of ca. 50 mV, which should equally effect the open circuit cell voltage. These results indicate in general the high purity conditions required for MEA preparation and the humidified feed-streams for PEMFC's. In addition to the kinetic effect of Cl^- adsorbed on the supported metal catalyst particles, its enhancement of the H_2O_2 production will be deleterious to the stability of perfluorinated membranes and ionomers in the catalyst layers (*e.g.*, Nafion membranes and ionomers), which are known to degrade in the presence of peroxide radicals. This does not only apply to the oxygen electrode, but also to the anode side which is exposed to oxygen either *via* O_2 crossover through thin *state-of-the-art* membranes (*e.g.*, GoreSelect or Nafion 112) or from air-bleed oxygen used for reformate operation (note when using air-bleed oxygen is present in a drastically over-stoichiometric concentration).

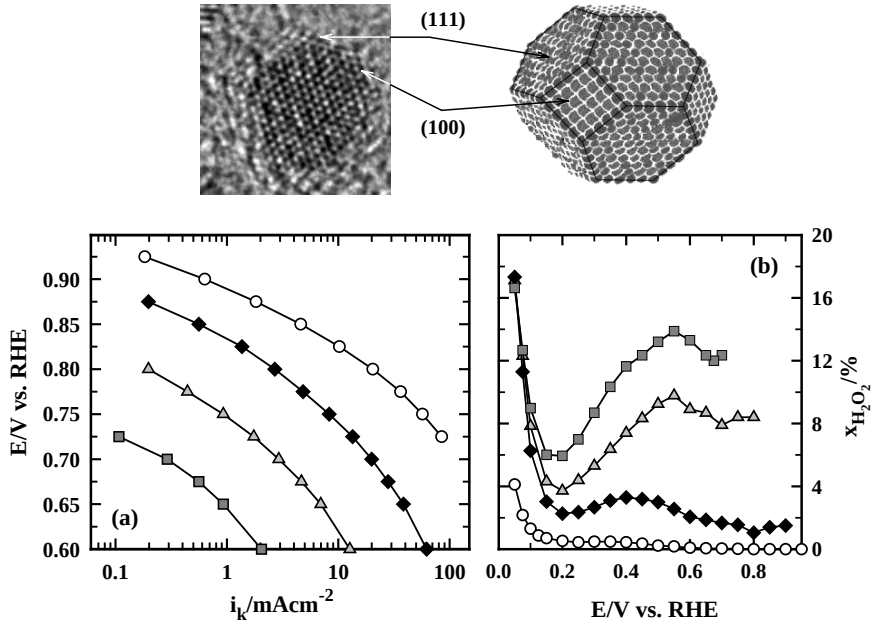

Fig. 3 **(a)** Tafel plots for the ORR on Pt/Vulcan in 0.5 M $HClO_4$ (white circles) and after addition of 10^{-4} M Cl^- (black diamonds), 10^{-3} M Cl^- (gray triangles), and 10^{-2} M Cl^- (gray squares). **(b)** Fraction of peroxide formed during the ORR in the presence of chloride. Notation as in (a). Top panel: High resolution TEM micrograph of a representative Pt particle and the proposed cubooctahedral shape.

3.4 Effects of "Air Bleed"

Previous work by Gottesfeld *et al.*, [43] has shown that bleeding of 0.4-2% oxygen into the CO-contaminated hydrogen can completely correct for deleterious effects of 5–100 ppm CO with a conventional Pt catalysts (0.4 mg/cm^2) in PEMFC. However many important questions regarding the air bleeding function are still unanswered. In order to get some new insights about the cleansing the anode catalysts by oxygen bleeding, the ORR was studied on

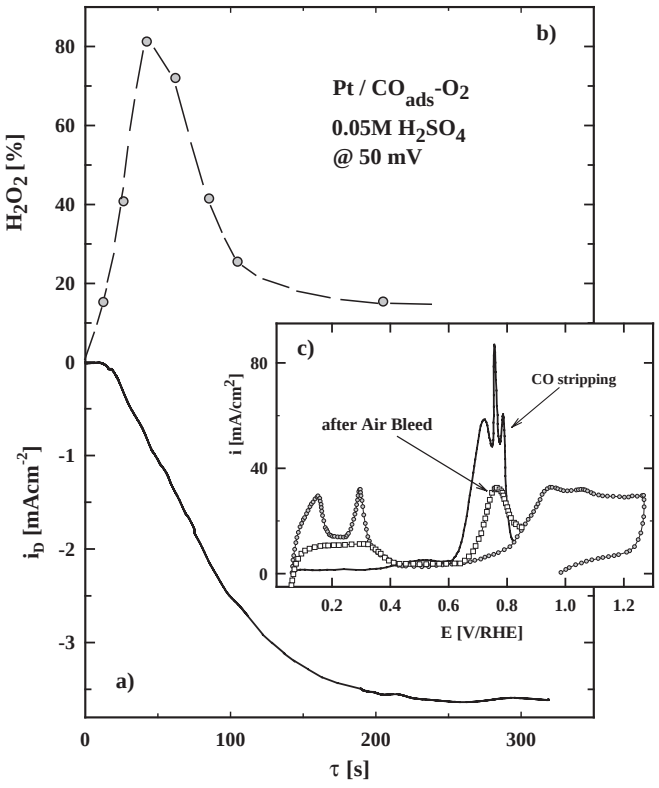

Fig. 4 **(a)** Potentiostatic oxygen reduction on a polycrystalline Pt electrode covered by 1 ML of CO_{ad} at 0.05 V. **(b)** Fraction of peroxide formed during the potentiostatic ORR on the CO-covered Pt surface. (0.05 M H_2SO_4, 0.05 V, 1600 rpm, 293 K). **(c)** Stripping of a CO_{ad} ML on polycrystalline Pt (dashed line) and of the remaining CO_{ad} after O_2 exposure in (a) (solid line). The Pt base CV is shown as a reference (dotted line).

a CO covered polycrystalline electrode. In these experiments, CO is adsorbed by holding the potential at 0.05 V in CO-saturated solution for 5 min followed by purging the solution with Ar to completely remove CO from solution. The transient current for the ORR on CO-covered Pt was recorded at 0.05 V, Figure 4a. The amount of peroxide produced on the disk electrode was monitored at the ring electrode (figure 4b). Figure 4 shows that on CO-covered surface a significant amount of peroxide is produced a short time after the introduction of O_2 (no CO present in solution!), then the production of peroxide drops away to a small but constant rate of ca 20 %. We note that under the same experimental condition only ca. 3–5% of peroxide was produced on the CO-free platinum surface. This enhanced production of peroxide on the Pt-CO_{ad} surface suggests that O_2 is *not* capable to completely oxidize CO, and consequently the remaining CO can effectively block the pair of sites required for the peroxide decomposition. To confirm this, O_2 was replaced by Ar and the stripping voltammetry of CO was recorded, see Figure 4c. Unexpectedly, we found that CO was indeed still present on the surface since CO stripping peak was clearly resolved at ca 0.8 V. The coverage of CO was ca. 40% of one corresponding for a surface fully covered by CO but never exposed to O_2 (insert of Figure 4). The fact that CO_{ad} cannot be completely oxidized by O_2 is a surprising result. Although the same effects were found for our unpublished Pt-Ru-CO and Pt-Sn-CO systems and a Pt/Vulcan high surface area catalyst, it is not possible unambiguously to propose a reaction mechanism for the "cleansing" of CO adsorbed on these metallic surfaces, *e.g.*, it may involve both chemical and electrochemical reactions.

4 ORR on bimetallic surfaces

In this section, we review recent progress in the fundamental science of the electrocatalysis of the ORR on Pt bimetallic surfaces. Bimetallic electrodes can be prepared in a number of ways. In this section, the focus will be on bimetallic platinum single crystal surfaces that are created by: the underpotential deposition (UPD) method, the classical metallurgical method and deposition of pseudomorphic metal films. The UPD adlayer is forming stable bimetallic surfaces only in the presence of the corresponding soluble cations. For the purpose of this review, the effects of Cu_{upd} on the ORR will briefly be discussed. The rate of the ORR will also be summarized on metallurgically prepared Pt-Co and Pt-Ni alloy surfaces. These results will, then, be compared with the kinetics on the supported Pt-Co catalysts. Because pseudomorphic Pd films supported on platinum single crystal surfaces has recently received considerable attention in surface electrochemistry, the ORR on the Pt(hkl)-Pd will be summarized as a model system.

4.1 Pt(hkl)- Cu_{upd} system

The effects of Cu_{upd} on the ORR at the Pt(100) interface in 0.05 M H_2SO_4 and 0.05 M H_2SO_4 +10^{-3} M Cl^- are shown in Figure 5. For comparison, the polarization curves for the ORR on Pt(100) in Cu^{2+}-free solutions under the same experimental conditions are shown as dotted curves. Clearly, in a solution containing Cu^{2+} ions the ORR is strongly inhibited in both Cl^--free (Figure 5b) and Cl^--containing solutions (Figure 5e). Very similar behavior was also observed on a polycrystalline electrode [44,45] and Pt(111) [17,46] in different acid solutions. Given that the kinetics of Cu UPD is a rather slow process, the ORR currents at the Cu_{upd}-modified surfaces are also measured under steady state conditions, see the closed circles in Figure 5b and e. In these experiments, the ORR is more inhibited than in the potentiodynamic experiments. As shown in Figure 5, the deactivation is more pronounced in the presence of Cl^- ions, presumably due to stronger interaction of specifically adsorbed chloride (Cl_{ad}) than bisulfate ($H_2SO_{4(ad)}$) anions with the Pt-Cu_{upd} surface. Note that at the Pt-Cu_{upd}-Cl_{ad} interfaces the inhibition of the ORR is observed at relatively small surface coverages by Cu_{upd}, for comparison see polarization curves and corresponding potential dependent surface coverage by Cu_{upd} ($\Theta_{Cu,upd}$), Fig. 5a and 5d. Recently, we suggested that the deactivation at Cu_{upd}-modified platinum single crystal surfaces arise due primarily to an enhanced anion adsorption on platinum atoms adjacent to Cu_{upd} atoms. This mechanism explains the anomalously large inhibition of the ORR and the HOR by a very small amount

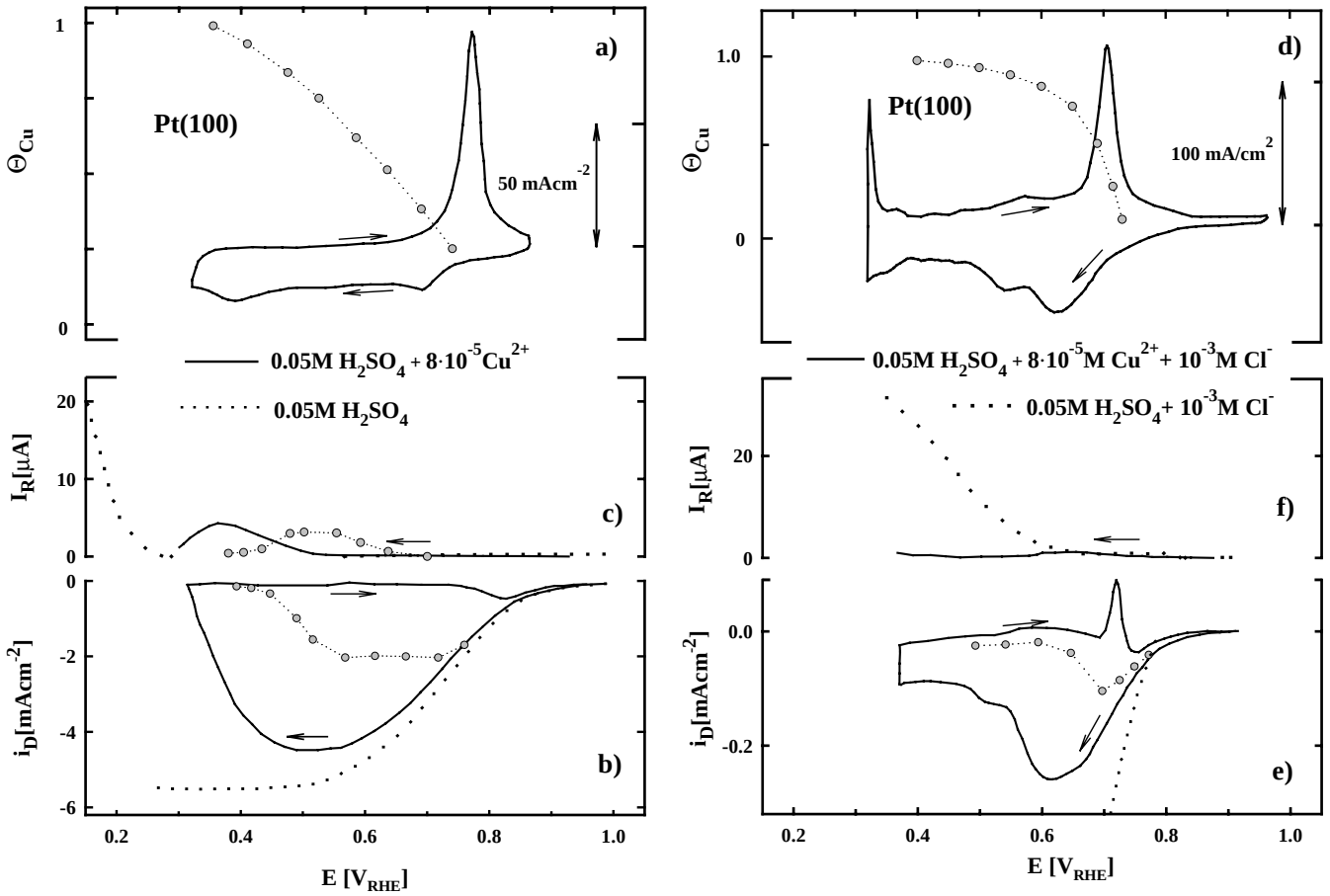

Fig. 5 **(a)** CV of Pt(100) in 0.05 M H_2SO_4 + 8·10^{-5} M Cu^{2+} and the Cu_{upd} adsorption isotherm (gray circles) **(b)** ORR on Pt(100) in 0.05 M H_2SO_4 + 8·10^{-5} M Cu^{2+} at 50 mV/s (solid line) and under potentiostatic conditions (gray circles). The ORR on Pt(100) in pure 0.05 M H_2SO_4 (dotted line) is shown for reference **(c)** Ring currents for peroxide detection, same notation as in (b). **(d)** CV of Pt(100) in 0.05 M H_2SO_4 + 8·10^{-5} M Cu^{2+} + 10^{-3} M Cl^- and the Cu_{upd} adsorption isotherm (gray circles) **(e)** ORR on Pt(100) in 0.05 M H_2SO_4 + 8·10^{-5} M Cu^{2+} + 10^{-3} M Cl^- at 50 mV/s (solid line) and under potentiostatic conditions (gray circles). The ORR on Pt(100) in pure 0.05 M H_2SO_4 for 2500 rpm (dotted line) is shown for reference. **(f)** Ring currents for peroxide detection, same notation as in (e). 50 mV/s, 293 K.

of Cu_{upd}. It is also interesting that under the negative going sweep direction the ring current is a very small fraction of the disk current, *i.e.*, is close to 3%, suggesting that a 4e$^-$ reaction pathway is still operative at Cu_{upd}-modified platinum single crystals. The physical model that appears to rationalize this result is one in which the active sites for adsorption of molecular O_2 are a small number of platinum islands created each time desorption of anions takes place from Cu_{upd}-unmodified platinum sites [22].

4.2 Pt-Co and Pt-Ni bimetallic surfaces

Several investigations have been carried out to determine the role of alloying in the electrocatalytic activity of Pt for the ORR (detailed review in ref. [5]). A definitive determination, however, remains elusive. Luczak et al., for example, found an increase in mass activity of a factor 1.5 to 2.5 when using PtCoCr or PtCr instead of pure Pt [9,47,48] whereas Beard et al. [49] and Glass et al. [50] found no change for PtCo and PtCr, respectively. Furthermore, Mukerjee *et al.*, [51] showed that five binary Pt-M alloy electrocatalysts (M = Cr, Mn, Co, and Ni) supported on carbon produced some enhancement in the kinetics (factor of 3-5) of the ORR relative to "standard" supported Pt catalyst. One of the difficulties in determining the effect of alloying components using supported catalysts is that the activity of a pure Pt supported catalysts can have a wide range of values depending on its microstructure and/or method of preparation. The intrinsic activity of Pt for the ORR depends on *both* particle shape and size [6,41], *i.e.*, there is not a single value of the specific activity even when normalized by Pt surface area. Since the alloyed Pt catalysts particles may not have either the same particle size or shape as the Pt catalysts to which they are compared, a simple comparison of activity normalized either by mass or surface area is insufficient to identify a true alloying effect. A more detailed discussion of this point, specifically in the case of Pt-Co catalysts, can be found in ref. [52]. These complexities of supported catalysts reinforced the need for using well-characterized materials to identify the fundamental mechanisms at work in electrocatalysis. As we demonstrate below, significant im-

provement of the ORR catalyses on Pt based alloy systems will require the inhibition of Pt-OH formation beyond 0.8 V.

4.2.1 Bulk alloy surfaces

Most recently, the intrinsic catalytic activity of Pt_3Ni and Pt_3Co alloy catalysts was studied in our laboratory with model bulk alloys characterized in UHV [17,53]. Figure 6 summarizes results for the ORR on UHV prepared and characterized bulk Pt_3Ni and Pt_3Co alloy catalysts in 0.1 M $HClO_4$ (note, on both samples the surface composition equals the bulk composition, as deduced by LEIS [17]). Pure polycrystalline Pt is also shown as a reference. As shown in Figure 6, the activity at 333 K increases in the order Pt_3Co > Pt_3Ni > Pt, the catalytic activity of Pt_3Co alloy being *ca*. 25mV improved with respect to the ORR on pure Pt. It should also be noted that similar small amounts of peroxide are detected on the ring electrode on all three surfaces during the ORR in perchloric acid solution. Interestingly, the Tafel slope (90 – 110 mV/dec) and the activation energy (20 to 25 kJ/mol) discerned for pure Pt is almost the same with values obtained for Pt_3Ni and Pt_3Co bimetallic surfaces. The fact that essentially the same kinetic parameters are assessed from the analyses implies that the reaction mechanism on Pt_3Ni and Pt_3Co alloy surfaces is the *same* as one proposed for pure Pt, *i.e.*, a "series" $4e^-$ reduction. Because the (chemical) rate constant K and the two exponential terms are essentially identical for all three systems the difference in the ORR kinetics must lie in the pre-exponential term, the $(1 - \Theta_{ad})$ term in equation 1. As demonstrated for Pt(hkl) [4], in perchloric acid electrolyte this term is primarily determined with the potential dependent surface coverage of the OH_{ad} species. As one can see from Figure 6, the catalytic effect of this term is ca.1.5-2; consistent with the shift of ca. 50 mV in oxidation potential. It is not clear why Ni and Co in the Pt surface would cause the shit in the oxidation potential of the Pt surface. One plausible explanation is that the adsorption of OH_{ad} *on* the Pt sites is modified by oxygenated species that are adsorbed on the alloying components. As for Pt-O interaction in UHV, the isosteric heat of adsorption of OH_{ad} on Pt sites (the surface coverage) surrounded by "oxide" covered Ni and Co atoms may significantly be reduced primarily from lateral repulsive interactions, and to much lesser extent the occupation of different adsorption sites. Therefore, being oxidized at much lower potentials then Pt, it appears that Ni and Co atoms may serve as "sacrificial" elements in Pt-Ni and Pt-Co alloys. Theoretical aspects of the relationships between the electronic structure and reactivity are, however, required in order to understand the trends in atomic/molecular chemisorption energies of oxygen containing species on Pt-Ni and Pt-Co bimetallic surfaces.

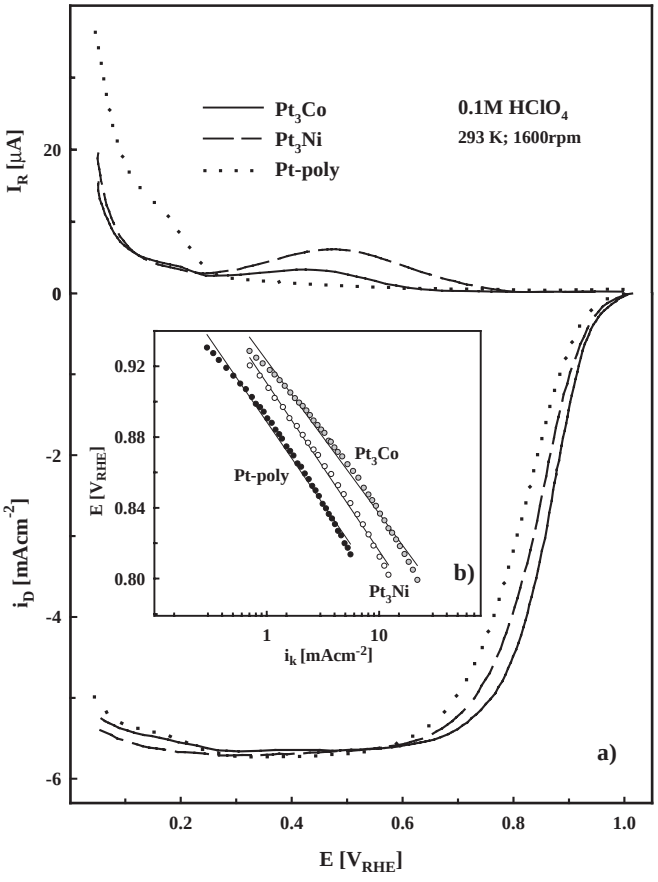

Fig. 6: **(a)** ORR on polycrystalline Pt (dotted line), Pt_3Ni (dashed line), and Pt_3Co (solid line) in 0.1 M $HClO_4$ at 293 K (20 mV/s). upper panel: Ring currents for peroxide detection. **(b)** Mass-transport corrected Tafel plots deduced from the polarization curves in (a) for Pt (black circles), Pt_3Ni (white circles) and Pt_3Co (gray circles).

4.2.2 Supported catalysts

In this section, we review some of experimental results for the ORR obtained on supported platinum and Pt alloy catalysts. The presentation here is restricted to a relatively brief overview, further details, including experimental procedure, can be found in references cited. As recently shown by Paulus *et al.*, [23], base voltammetry (Figure 7a) and complementary TEM analysis allow the determination of the particle size distribution and the estimation of the surface composition. These analyses can provide an adequate, although not necessarily complete characterization of the microstructure of the catalyst that we could use to correlate the surface activity of Pt-Co nanoparticles with the model bulk alloy surfaces shown in the preceding section. A low magnification of TEM image of

Tab. 1 Characterization of Pt/Vulcan and PtM/Vulcan catalysts.

Catalyst	atomic density per electrode [nmol/cm^2]	surface atomic density [nmol/cm^2]	Charge H_{upd}-region [mC/cm^2]	Active (Pt) surface atoms [nmol/cm^2]	Estimated Surface composition
Pt/Vulcan	72.4	21.7	1.97	20.4	(100%)
PtCo/ Vulcan	111.4	27.8	0.72	7.5	27%
Pt_3Co/ Vulcan	87.8	22.0	1.40	14.5	66%
Pt_3Ni/ Vulcan	87.8	22.0	1.52	15.8	70%

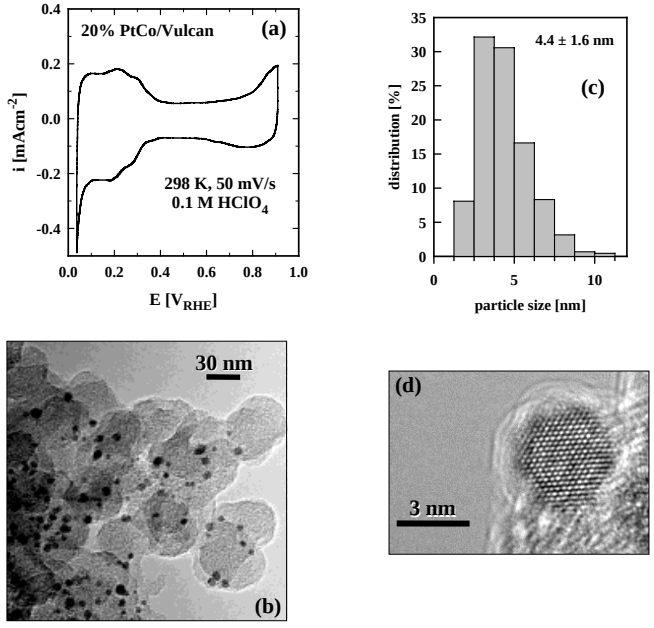

Fig. 7: **(a)** Base CV of 20 %PtCo/Vulcan (1:1) in 0.1 M $HClO_4$ (50 mV/s, 298 K). **(b)** Low Resolution TEM micrograph for the PtCo/Vulcan catalyst. **(c)** Particle size distribution for PtCo/Vulcan. **(d)** High resolution TEM micrograph of a single PtCo particle.

Pt-Co catalyst, shown in Figure 7b, illustrates that the distribution of metal particles on the carbon support is rather uniform. The histogram for the particle size distribution (Figure 7c), which included analyses of several different regions of the catalysts, revealed that the average particle size is *ca.* 4.4 nm. Finally, the x-ray emission energy filtering imaging technique enabled us to determine that the catalysts dispersed on the support are completely alloyed. This was achieved by comparing the micrographs and the cobalt map images (not shown). For details the reader is referred to reference [23,54]. The cyclic voltammogram for PtCo/Vulcan and Pt/Vulcan is presented in Figure 7a. Figure 7 shows that the voltammetry of PtCo/Vulcan has a suppressed pseudocapacitance in the H_{upd}-region with respect to Pt/Vulcan electrode, clearly indicating that the charge associated with H_{upd} depends on the availability of Pt surface atoms. As described in ref. [20,23], the electrochemical active surface areas for the catalysts were determined by integrating the area in the H_{upd}-region. The H_{upd}-charges are listed in table 1 together with the resultant number of Pt-surface atoms for all investigated high surface area catalysts.

The best form of representation of catalytic activity on supported catalysts is by comparing the kinetic currents for the ORR at three different potentials in the form of histograms, Figure 8. These graphs clearly show that the kinetics of the ORR on supported Pt and platinum alloy catalysts is dependent on the nature of the alloying component, *e.g.*, Pt < PtNi < PtCo, and the surface composition Pt_3Co < PtCo. As for bulk alloy surfaces in Figure 6, a small amount of peroxide was detected on the ring electrode on all alloy surfaces, implying that the reaction pathway for the ORR on supported

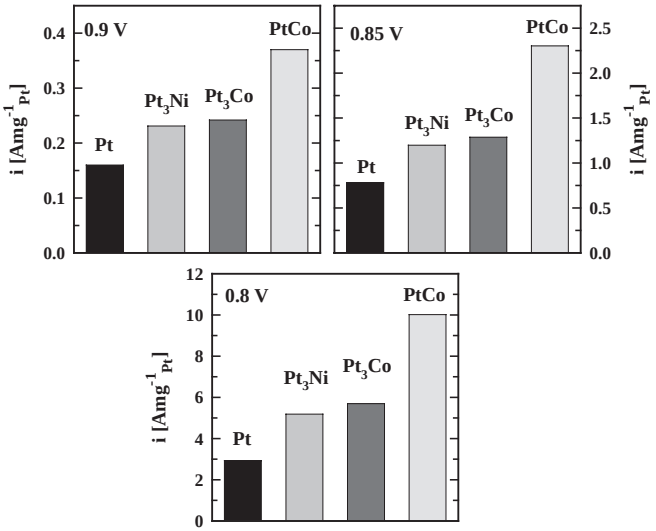

Fig. 8: Comparison of the mass-transport corrected mass-specific current densities at 0.9, 0.8%, and 0.8 V obtained on Pt/Vulcan, Pt_3Ni/Vulcan, Pt_3Co/Vulcan, and PtCo/Vulcan.

catalysts is the *same* as one proposed for bulk alloys, e.g., a "series" $4e^-$- reduction pathway. Further comparison of the kinetic parameters of the bulk and high surface area catalysts provide a rational for the enhanced catalytic activity of supported PtNi and PtCo catalysts. Because both the activation energy (ca. 20–25 kJ/mol) and the Tafel slopes (ca. 90–110 mV/dec) for high-surface-area catalysts are essentially identical to that observed on the bulk electrodes in Figure 6, one can propose that the differences in the kinetics of the ORR is

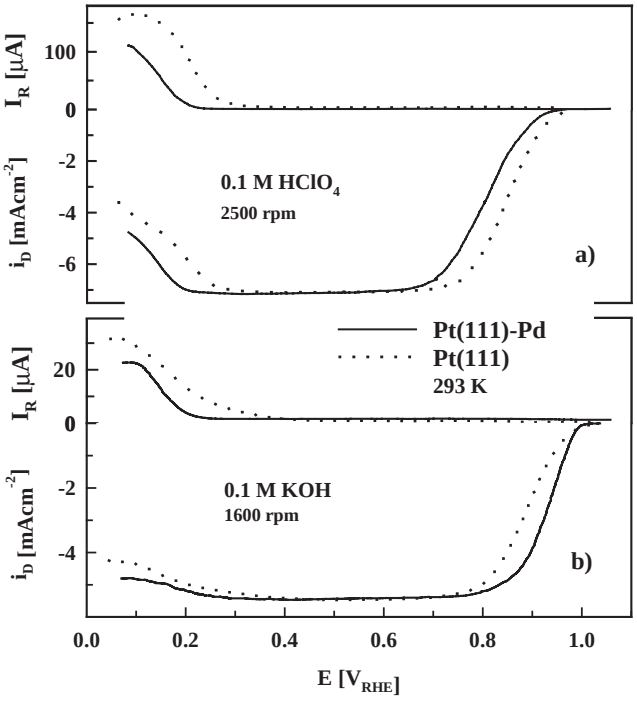

Figure 9: Disk and Ring currents for the ORR on Pt(111)-1 ML Pd (solid line) in **(a)** 0.1 M $HClO_4$ and **(b)** 0.1 M KOH. The dotted line represents unmodified Pt(111) under the same conditions. 50 mV/s, 293 K.

determined with the $(1–\Theta_{ad})$ term in equation 1, *e.g.*, the reduced adsorption of OH_{ad} *on* Pt sites surrounded by "oxide"-covered Ni and Co atoms. To conclude this section, we emphasize that the PtCo alloy is a promising catalyst for the ORR for two reasons: (i) the amount of Pt in air cathode fuel cells may substantially be reduced (by ca. 25-50 %), and the activity is significantly improved with respect to the ORR on pure Pt.

4.3 Pt(111)-Pd systems

Figure 9 summarizes a family of polarization curves for the ORR on the Pt(111)-Pd electrode in O_2-saturated 0.1 M $HClO_4$, and 0.1 M KOH solutions along with representative polarization curves recorded in the same solution but on unmodified Pt(111). Figure 8a shows that in 0.1 M $HClO_4$ the ORR is inhibited at the Pt(111)-Pd surface, probably due to stronger interaction of Cl_{ad} (which is present as trace impurity in perchloric acid [55]) with the Pd film than with an unmodified Pt(111) electrode [18]. The decrease in the rate of the ORR at the disk electrode is, however, *not* associated with peroxide detection on the ring electrode, indicating that pairs of Pd sites are always available for the breaking of the O-O bond. This implies that the direct $4e^-$ path is operative in this potential region. In contrast to perchloric acid solution, the Pt(111)-Pd electrode shows a unique catalytic activity for the ORR in alkaline solution. A critical assessments of this work shows that the rate of the ORR on Pt(111)-Pd electrode is improved by factor of two relative to unmodified Pt(111), Figure 8b. Keeping in mind that the Pt(111) electrode in KOH *was* the most active catalyst for the ORR, the catalytic improvement observed on the Pt(111)-Pd surface is an extremely important new observation which may help in the quest for developing better ORR catalysts. The fact that the activity of Pt(111)-Pd electrode is significantly higher in KOH then in $HClO_4$ implies that the major deactivation in acid electrolytes arise from strong interaction of specifically adsorbing anions with the (111) surface. Therefore, the strong adsorption of anions may hinder the adsorption of molecular oxygen and/or reduce the likelihood of its dissociation. As a result, the kinetics of the ORR on Pt(111)-Pd relative to clean Pt(111) is mostly determined by the pre-exponential $(1–\Theta_{ad})$ term in equation 1. This term is determined by the modification of surface electrochemical properties (the work function and thus the potential of zero charge) caused by charge redistribution upon forming the Pt-Pd bond. More details about the ORR on the Pt(111)-Pd surface, including the effects of H_{upd} on the kinetics, may be found in references [18].

5 Summary

In this review we summarize selectively recent progress, primarily from our laboratory, in the development of the ORR catalysis on well-defined surfaces. The focus was on two types of metallic surfaces: platinum single crystals and bimetallic surfaces based on platinum. The single crystal results provided insight into the effects of the platinum structure on the kinetics of the ORR, and created a fundamental link between the specific activity of Pt (rate per unit area) and particle size (for various particle shapes). The results show that the structure-sensitive kinetics of the ORR arise primarily due to structure sensitive adsorption of anions of supporting electrolyte. The ORR on Pt(hkl)-Cl_{ad} and Pt(hkl)-Cu_{upd} electrodes is strongly inhibited. The single crystal results showed that Cl_{ad} has two effects in the kinetics of the: (i) Cl_{ad} acts as a site-blocking species which is reducing the number of active sites for the adsorption of O_2 molecules and (ii) Cl_{ad} is affecting the number of sites required for the breaking of the O-O bond. The same mechanism of action was used to explain the effect of Cl^- on the rate of the ORR on supported Pt catalysts. The physical model that appears to rationalize a strong inhibitive effect of Cu_{uod} is one in which the active sites for adsorption of molecular O_2 are a small number of platinum islands created each time desorption of anions takes place from Cu_{upd}-unmodified platinum sites.

The knowledge of the electrocatalysis of the ORR on model bimetallic surfaces on Pt-Ni and Pt-Co bulk alloys has been used to resolve the enhanced ORR kinetics on supported Pt-Ni and Pt-Co catalysts. We proposed that significant improvement of the ORR catalyses on Pt based alloy systems appears primarily due to the inhibition of Pt-OH formation *on* Pt surrounded by "oxide"-covered Ni and Co atoms beyond 0.8 V.

The kinetics of the ORR on Pt(111) modified with Pd metal films is depending of anions of supporting electrolyte either reduced ($HClO_4$) or catalyzed (KOH). Keeping in mind that the Pt(111) electrode in KOH *was* the most active catalyst for the ORR, the catalytic improvement observed on the Pt(111)-Pd surface is an extremely important new observation which may help in the quest for developing better ORR catalysts.

Acknowledgments

This work was supported by the U.S. Department of Energy, the Office of Science, Basic Energy Sciences, Materials Sciences Division, and the Office of Advanced Transportation Technologies, Fuel Cell Systems, under contract DE-AC03-76SF00098.

References

[1] A. Damjanovic, in *Modern Aspects of Electrochemistry*, J.O.M. Bockris, B.E. Conway, Editors, p. 369, Plenum Press, New York (1969).

[2] M.R. Tarasevich, A. Sadkowski, E. Yeager, in *Comprehensive Treatise in Electrochemistry*, J.O.M. Bockris, B.E. Conway, E. Yeager, S.U.M. Khan, R.E. White, Editors, p. 301, Plenum Press, New York (1983).

[3] R.R. Adzic, in *Electrocatalysis*, J. Lipkowski, P.N. Ross, Editors, p. 197, Wiley-VCH, Inc., New York (1998).

[4] N.M. Markovic and P.N. Ross Jr., in *Interfacial Electrochemistry – Theory, Experiments and Applications*, A. Wieckowski, Editor, p. 821, Marcal Dekker Inc., New York (1999).
[5] A.J. Appleby, Catalysis Reviews, 4 (1970) 221.
[6] K. Kinoshita, *Electrochemical Oxygen Technology*, John Wiley & Sons, New Vork 1992.
[7] H.G. Petrow and R.J. Allen, *United States Patent 3, 992, 331,* filed 1974.
[8] K. Kinoshita, K. Routsis, J.A.S. Bett, Thermochimica Acta, 10 (1974) 109.
[9] F.J. Luczak and D.A. Landsman, *United States Patent No. US 4.447.506,* filed 1984.
[10] F.J. Luczak and D.A. Landsman, *United States Patent No. 4.711.829,* filed 1987.
[11] P. Stonehart, *United States Patent No. US 5.593.934,* filed 1997.
[12] E. Auer, A. Freund, T. Lehmann, K.-A. Starz, R. Schwarz, U. Stenke, *German Patent No. DE 197 21 437 A1,* filed 1998.
[13] J. Clavilier, A. Rodes, K. El-Achi, M.A. Zamakhchari, J. Chim. Phys., 88 (1991) 1291.
[14] N.M. Markovic, M. Hanson, G. McDougal, E. Yeager, J. Electroanal. Chem., 241 (1986) 309.
[15] N.M. Markovic, H.A. Gasteiger, P.N. Ross, J. Phys. Chem., 99 (1995) 3411.
[16] H.A. Gasteiger, P.N. Ross, E.J. Cairns, Surf. Sci., 293 (1993) 67.
[17] V. Stamenkovic, T.J. Schmidt, N.M. Markovic, P.N. Ross Jr., J. Phys. Chem. B, (2001)
[18] V. Climent, N.M. Markovic, P.N. Ross, J. Phys. Chem. B, 104 (2000) 3116.
[19] T.J. Schmidt, H.A. Gasteiger, G.D. Stäb, P.M. Urban, D.M. Kolb, R.J. Behm, J. Electrochem. Soc., 145 (1998) 2354.
[20] U.A. Paulus, T.J. Schmidt, H.A. Gasteiger, R.J. Behm, J. Electrochem. Soc., (1999)
[21] V. Stamenkovic, N.M. Markovic, P.N. Ross Jr., J. Electroanal. Chem., 500 (2000) 44.
[22] V. Stamenkovic and N.M. Markovic, Langmuir, 179 (2001) 2388.
[23] U.A. Paulus, G.G. Scherer, A. Wokaun, T.J. Schmidt, V. Stamenkovic, V. Radmilovic, N.M. Markovic, P.N. Ross, J. Electroanal. Chem., (2001)
[24] T.J. Schmidt, U.A. Paulus, H.A. Gasteiger, R.J. Behm, J. Electroanal. Chem., (2001)
[25] F. Will, J. Electroanal. Chem., 112 (1965) 451.
[26] I.M. Tidswell, N.M. Markovic, P.N. Ross, Phys. Rev. Lett., 71 (1993) 1601.
[27] I.M. Tidswell, N.M. Markovic, P.N. Ross, J. Electroanal. Chem., 376 (1994) 119.
[28] H. Wroblowa, Y.C. Pan, J. Razumney, J. Electroanal. Chem., 69 (1976) 195.
[29] B.N. Grgur, N.M. Markovic, P.N. Ross Jr., Can. J. Chem., 75 (1997) 1465.
[30] N.M. Markovic, H.A. Gasteiger, B.N. Grgur, P.N. Ross, J. Electroanal. Chem., 467 (1999) 157.
[31] M.R. Tarasevich, Electrochimiya, 9 (1973) 578.
[32] F. Uribe, M.S. Wilson, T. Springer and S. Gottesfeld, in D. Scherson, D. Tryk, M. Daroux, X. Xing (Eds.), Proceedings of the Workshop on Structural Effetcs in Electrocatalytsis and Oxygen Electrochemistry, **PV 92-11,** p. 494, The Electrochemical Society, Pennington, NJ, 1992.
[33] F. EL Kadiri, R. Faure, R. Durand, J. Electroanal. Chem., 301 (1991) 177.
[34] N.M. Markovic, R.R. Adzic, B.D. Cahan, E. Yeager, J. Electroanal. Chem., 377 (1994) 249.
[35] N.M. Markovic, H.A. Gasteiger, P.N. Ross, J. Phys. Chem., 100 (1996) 6715.
[36] T.J. Schmidt, B.N. Grgur, N.M. Markovic, P.N. Ross Jr., J. Electroanal. Chem., 500 (2001) 36.
[37] B.N. Grgur, N.M. Markovic, P.N. Ross Jr., Langmuir, 13 (1997) 6370.
[38] N.M. Markovic, N.S. Marinkovic, R.R. Adzic, J. Electroanal. Chem., 241 (1988) 309.
[39] M. Peuckert, T. Yoneda, B. Dalla, M. Boudart, J. Electrochem. Soc., 13 (1986) 944.
[40] M. Sattler and P.N. Ross, Ultramicroscopy, 20 (1986) 21.
[41] N.M. Markovic, H.A. Gasteiger, P.N. Ross, J. Electrochem. Soc., 144 (1997) 1591.
[42] T.J. Schmidt, U.A. Paulus, H.A. Gasteiger, N. Alonso-Vante, R.J. Behm, J. Electrochem. Soc., (1999)
[43] S. Gottesfeld, *United States Patent No. 4,910,099,* filed 1990.
[44] G. Kokkinidis and D. Jannakoudakis, J. Electroanal. Chem., 162 (1984) 163.
[45] S.A.S. Machado, A.A. Tanaka, E.R. Gonzales, Electrochim. Acta, 36 (1991) 1325.
[46] T. Abe, G.M. Swain, K. Sashikata, K. Itaya, J. Electroanal. Chem., 382 (1995) 73.
[47] C.A. Lucas, N.M. Markovic, P.N. Ross, Phys. Rev. B, 55 (1997) 7964.
[48] F.J. Luczak and D.A. Landsman, *United States Patent No. US 4.677.092,* filed 1987.
[49] B. Beard and P.N. Ross Jr., J. Electrochem. Soc., 137 (1990) 3368.
[50] J.T. Glass, G.L. Cahen, G.E. Stoner, J. Electrochem. Soc., 134 (1987) 58.
[51] S. Mukerjee and S. Srinivasan, J. Electroanal. Chem., (1993) 201.
[52] P.N. Ross Jr., in *Electrocatalysis*, J. Lipkowski, P.N. Ross Jr. Editors, p. 43, Wiley-VCH, Inc., New York (1998).
[53] P.N. Ross, N.M. Markovic, T.J. Schmidt and V. Stamenkovic, in Fuel Cell for Transportation FY 2000 Annual Report, US Department of Energy, Washington, DC, 2000.
[54] V. Radmilovic, in preparation, (2001)
[55] N.M. Markovic and P.N. Ross, J. Electroanal. Chem., 330 (1992) 499.